Prompt Fission Neutron Investigation in $^{235}U(n_{th},f)$ and $^{252}Cf(sf)$ Reactions

Shakir Zeynalov, *Pavel* Sedyshev, *Valery* Shvetsov and *Olga* Sidorova

Joint Institute for Nuclear Research, 141980 Dubna Moscow region, Russia

Abstract. The prompt neutron emission in thermal neutron induced fission of ^{235}U and spontaneous fission of ^{252}Cf was investigated by using digital signal electronics. The goal was to check a new revised data analysis software with fission fragment (FF) kinetic energy corrections after prompt fission neutron (PFN) emission. The revised software was used to reanalyze old data measured in EC-JRC-IRMM, where $^{252}Cf(sf)$ reaction was investigated. Both measurements were done using similar twin Frisch grid ionization chamber for fission fragment detection with equivalent NE213 fast neutron detector. About $0.5*10^6$ FF with PFN coincidences have been analyzed in both measurements. The fission fragment kinetic energy, mass and angular distribution were investigated along with prompt neutron time of flight and pulse shape analysis using a six channel synchronous waveform digitizer (WFD) with sampling frequency of 250 MHz and 12 bit resolution in the $^{235}U(n_{th},f)$ reaction. Similar WFD with sampling frequency of 100 MHz was used for PFN investigation in $^{252}Cf(sf)$ reaction. These two experiments were considered as a reference for further investigations with a new setup composed of position sensitive ionization chamber to detect FF and an array of 32 liquid scintillators recently constructed in Dubna to detect neutrons.

1 Introduction

The nuclear fission is considered as the process of a charged drop evolving under the competition between attractive nuclear and repulsing coulomb forces, leading eventually to the split of the nucleus mainly into two parts of comparable masses. The main part of FF excitation energy is released by the prompt fission neutrons, emitted by FF after full acceleration by coulomb forces. The experimental investigations of various characteristics of PFN emission is needed to understand the nuclear fission dynamics from the scission point down to rupture. One of the interesting observation is the increasing $\bar{\nu}(A)$ from the heavy fragment with increase of the excitation energy of the fissioning system [1] which has still no clear explanation. Therefore the systematic study of correlations between fragments and neutrons characteristics is needed. The studies of PFN emission in fission induced by neutrons from energies extending from resonances up to a few MeV could possibly contribute to better understanding the mechanism of PFN emission from the excited FF. The experiments on sub-barrier fission, induced by thermal neutrons are of particular interest because no measurements were done so far on mass and energy distributions for this systems [2]. In this work we report results of PFN investigation in thermal neutron-induced fission of ^{235}U and spontaneous fission of ^{252}Cf. The main goal of the experiments was the feasibility check of the apparatus and the data analysis procedure.

2 Experimental Setup and FF data analysis

A convenient way to study of PFN emission in neutron-induced fission is to use a conventional twin back-to-back ionization chamber, with two chambers sharing a common cathode such as the one of Budtz-Jorgensen and Knitter [3]. The cathode was made from a thin conductive foil and at the same time served as backing for the fissile deposit. For binary fission events two complementary FF are simultaneously detected in the two independent chambers. Free electrons released by FF deceleration were inducing pulses on the chamber anodes and on the common cathode during drift along the applied externally electric field. The pulse height in each chamber was proportional to the corresponding FF kinetic energy and the pulse shape conveys information on the FF angle (Θ) in respect to the electric field applied in the direction of the normal to the cathode plane. From the correlated energies obtained in the above double-energy (2E) experiment, FF masses and velocities could be found in a similar way than exposed in [4]. If the fissile target is located on the common cathode and the fast neutron detector positioned at the certain distance along the normal to the target, the angle between FF and PFN emission would be equal to Θ. The PFN velocity may be determined from the known flight path and the measured time delay between cathode and neutron detector (ND) pulses. Measured FF and PFN velocity vectors then may be used for PFN emission kinematics. The PFN multiplicity distributions in respect to FF kinetic energy release and mass split may be reconstructed comparing of two sets of FF measurements. In the first experiment fission fragment mass and kinetic energy release should be evaluated from the measurement independent from ND. In the second experiment FF mass and kinetic energy release should be evaluated for the FF coincided with ND. The detailed information on PFN emission in fission is available from the measured dependence of the number $\nu(A,TKE)$ of PFN emitted by the FF with mass number A and TKE release of two fission fragments [3-4]. The late function allowed obtaining the averaged characteristics of $\nu(A)$ or $\nu(TKE)$ by integrating over respective variable, if the mass yield matrix - *Y(A,TKE)* is known:

$$\bar{\nu}(A)=\frac{\int_0^\infty \nu(A,TKE)Y(A,TKE)dTKE}{\int_0^\infty Y(A,TKE)dTKE},\quad \bar{\nu}=\int_0^\infty \nu(A,TKE)Y(A,TKE)dTKEdA,\ 200=\int_0^\infty Y(A,TKE)dTKEdA \tag{1}$$

Similar relation could be written for averaging over A:

$$\bar{\nu}(TKE)=\frac{\int_0^\infty \nu(A,TKE)Y(A,TKE)dA}{\int_0^\infty Y(A,TKE)dA},\quad \bar{\nu}=\int_0^\infty \nu(A,TKE)Y(A,TKE)dTKEdA,\ 200=\int_0^\infty Y(A,TKE)dTKEdA \tag{2}$$

$\nu(A),\nu(TKE)$ can be easily determined if the distributions of $\nu(A,TKE)$ and $Y(A,TKE)$ are known. The experimental method and data analysis procedure implemented in this work was adopted from Ref. [3], where it was described in detail. For each fission event the FF and PFN kinetic energies, FF masses along with the angle between PFN and FF motion should be determined. All this information can be used to reconstruct the PFN emission kinematics both in the laboratory (LF) and in the centre of mass (CMF) frames. The measurements were carried out using the experimental setup presented in Fig. 1 (on the right). Reaction kinematics is sketched in Fig. 1 (on the left). The experimental setup consisted of the twin back-to-back ionization chamber (TIC), which was designated for the measurements of FF kinetic energy release and the cosine of angle between fission axis and the cathode plane normal. The experimental data was collected using a digital pulse processing (DPP) system, consisting of six synchronous waveform digitizers (12 bit, 250 MS/sec). The FF energies and angles were obtained from the

chamber signal waveforms using DPP, realized in form of recursive procedures. The neutron energy was derived from time-of-flight (TOF) calculated as the delay between the

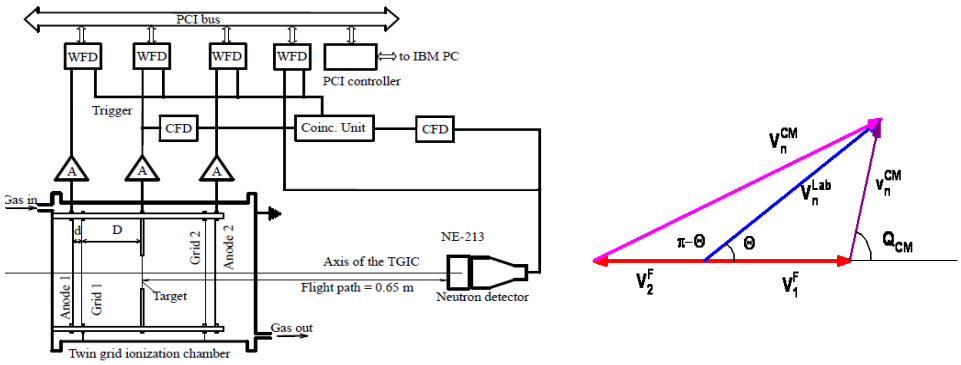

Fig. 1. Experimental setup(left). Vector diagram for PFN emission from FF (right)

cathode and the neutron detector pulses. The measured FF energy release should be corrected for energy losses in the target layer and target backing if the cosine of angle Θ is known. In this work anode current pulse waveform was derived from the output pulse of charge sensitive preamplifier and the pulse "centre of gravity" (T) calculated as described in Ref. [5]. The relation between T and the cos(Θ) was derived in Ref. [6] using Ramo-Shokley theorem and numerically calculated weighting potentials:

$$\cos(\Theta) = (T_{90} - T)/(T_{90} - T_0) \quad (3),$$

where the used variables have the following meaning: D-is the cathode-anode distance, d-is the grid-anode distance, σ-is the Frisch grid inefficiency value, $T_0 = T(\cos(\Theta) = 1)$, $T_{90} = T(\cos(\Theta) = 0)$. The below formula was used to correct anode signal pulse heights for grid inefficiency:

$$P_A^C = P_A/(1 - \sigma \cdot (1 - \frac{T}{T_{90}}) \cdot (1 + \frac{d}{2D})) \quad (4)$$

After the emission angle was calculated, the average anode pulse height versus 1/cos(Θ) was plotted for both chambers to find energy loss correction for FF detected in each chamber. The data sets are fitted as a linear function of 1/ cos(Θ), the slopes of which were assigned to energy loss correction in respective chamber. The correction for FF pulse height, caused by momentum transfer to working gas atoms by FF (non ionizing collisions) during its deceleration, is called pulse height defect (PHD). The PHD depends on the FF mass and kinetic energy and was corrected in data analysis using parameterization suggested in Ref. [6]:

$$E = \alpha \cdot PH + \beta + PHD(A_{post}, E_{post}) \quad (5),$$

where $E_{post}t$, A_{post} - FF kinetic energy and mass respectively after neutron emission. The fitting parameters α and β - are chosen to fit the values of TKE and the $\langle A_H \rangle$ as given in Ref. [4] p. 323.

3 Data analysis procedure

Measurement of PFN time-of-flight in present experiment was done using cathode pulse of TIC as a "T-zero" signal and the ND signal as "Stop" signal. The signals were digitized with 250 MHz sampling rate and stored during experiment for further off-line data analysis.

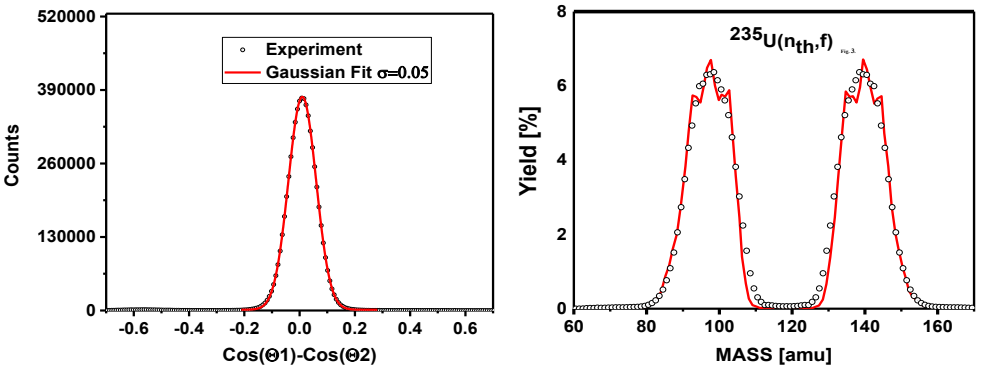

Fig. 2. Demonstration the precision of cos(Θ) measurement in the range 0.5<cos(Θ)<1.0 (on the left). Comparison of measured mass yield (dots) with data (solid line) taken from Ref.[4]. For calculations the successive approximation procedure to obtain pre-PFN emission mass described in Ref. [3] was used (on the right).

Time difference between these two signals was analyzed by implementing standard constant fraction time marking (CFTM) algorithm both to the cathode and to the ND waveforms.

The realization of the algorithm described in Ref. [9] was applied to the cathode waveform. The copy of the original signal is delayed by approximately 400ns of the cathode signal rise time (~1000 ns) and summed with scaled and inverted original signal. The "T-zero" time is assigned to the crossing point of resulting signal with time axis. The crossing point was calculated using parabola interpolation between two successive samples. The time mark for the ND signal was found in the similar way. It should be noted that to achieve the best timing resolution in CFTM realization one should convert sampled waveform to continuous form using Shannon's sampling formula [9]. In this study the PFN kinetic energy spectrum reconstruction was not needed, therefore the resolution ~2.5 ns achieved in this simple implementation was found sufficient for PFN analysis. The neutron multiplicity was estimated by counting the coincidence between cathode pulse and PFN signal of ND. Due to high gamma radiation background both from the target and surrounding materials the PFN counts needed to be separated from the gamma radiation using pulse shape analysis as described in Ref. [9].

The PFN detected by ND was mainly emitted from FF moving towards the ND, but the probability, that it was emitted by FF moving in opposite direction (complementary FF) was not zero and these events were considered as background. The background created by the complementary FF was investigated in Ref. [5] and was slightly modified in our approach. According to the reaction kinematics depicted in Fig. 1, the kinetic energy of the complementary FF in the CMF, must be much higher than the kinetic energy of the FF moving toward the ND. Bearing in mind the exponential drop of the PFN energy spectrum in the CMF, the contribution to the PFN from both FFs could be evaluated using the probabilities defined as:

$$W_x = 1/(1+\exp(E^x_{CM} - E^y_{CM})),$$
$$W_y = \exp(E^x_{CM} - E^y_{CM})/(1+\exp(E^x_{CM} - E^y_{CM})) \quad (6),$$

where W_x, W_y - are the probabilities of PFN emission with CM kinetic energies $E^{x,y}_{CM}$ of PFN from the forward FF and its complement respectively. A comparison of the mass distributions plotted using measured data and probabilities, defined by Eq. (6) are similar to

Ref. [3], where the background from the complementary fragments for ^{252}Cf(sf) was found to be small.

The angular distribution of PFN emitted in FF CM reference frame was homogeneous, proving that almost all of the PFN are emitted from fully accelerated FFs. The transformation from the LAB to CM reference frame was done using the following formula:

$$\cos(\Theta_{CM}) = (V_n^{Lab} \cdot \cos(\Theta_{Lab}) - V_1^F)/V_n^{CM} \quad (7)$$

4 Results of PFN analysis in ^{235}U(n_{th},f) reaction.

The PFN distribution was evaluated considering neutron emission from the fully accelerated FF, using the reference frame moving along with the FF towards the ND. We used the Jacobean factor and conversion formulae from CM to LAB reference frame as was described in Ref. [10]:

$$\bar{\nu}(A,TKE) == \int_0^\infty \frac{Yc(A,TKE,V_{LAB}) \cdot V_{CM} \cdot (V_{LAB} - V_F \cdot \cos(\Theta))}{\varepsilon(V_{LAB}) \cdot V_{LAB}^2} dV_{LAB} / Y(A,TKE) \quad (8),$$

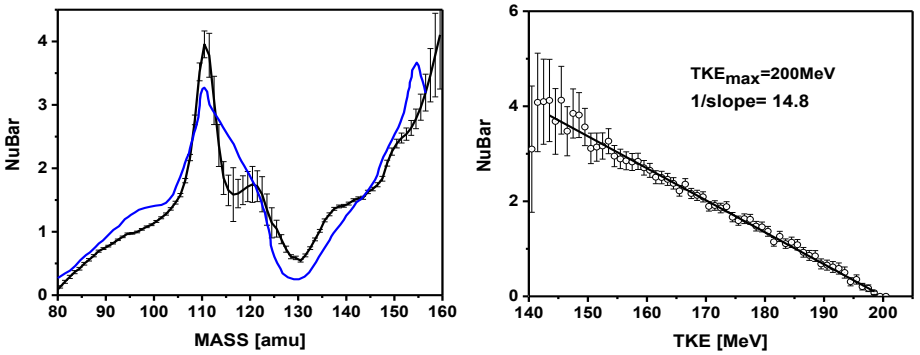

Fig. 3. The average PFN emission distribution mass dependence (black line), measured in ^{235}U(n_{th},f) reaction in comparison with data (blue line) from Ref. [7] (on the left). The average PFN emission distribution dependence on FF TKE, measured in ^{235}U(n_{th},f) reaction with TKE$_{max}$= ~200 MeV (on the right).

where $Y_C(A,TKE,V_{LAB})$ - the number of FF coincidences with ND, $\varepsilon(V_{LAB})$ - is the ND efficiency dependence on PFN velocity in LAB frame, V_{LAB} - the PFN velocity measured in LAB frame, V_F - FF fragment velocity in LAB frame, V_{CM} - is the PFN velocity in CM frame. The distribution $Y(A,TKE)$ was calculated without coincidence with ND as described above, but distribution $Yc(A,TKE,V_{LAB})$ was calculated with FF energy corrected due to FF recoil after PFN emission as described in Ref. [11]. Dependence of average PFN multiplicities on mass and TKE were evaluated using formulae (1,2) and plotted in Fig. 3.

It should be noticed that measurement of $\bar{\nu}(A)$ in ^{235}U(n_{th},f) was more complicated in comparison with ^{252}Cf(sf) due to very high peak to valley ratio in FF mass distribution for ^{235}U. Low statistics in the valley area of mass distribution makes data analysis very sensitive to background. This is why in this report we reanalyzed the data with the same data analysis software that was used in the analysis of the ^{235}U(n_{th},f) reaction. The test of

our data analysis procedure in ^{252}Cf(sf) reaction was necessary to have confidence in our results for ^{235}U(n_{th},f) which more precisely reproduced the mass distribution of the reaction. Our target was made on the polyamide backing with thickness of 35 μg/cm^2 and the sample layer thickness was ~50 μg/cm^2. Experiment was carried out on the IBR2 pulsed reactor with thermal neutron flux ~2*10^6 n/cm^2. The sample diameter was 60 mm.

5 Results of PFN analysis in ^{252}Cf(sf) reaction.

Measurement of PFN in spontaneous fission of ^{252}Cf was done in 2007-2009 at IRMM using an experimental setup similar to the one presented in Fig.1. The ionization chamber was absolutely identical to the chamber used in above reported study. The PFN detectors were the same size but in case of experiment with Cf-target the distance between target and PFN detector

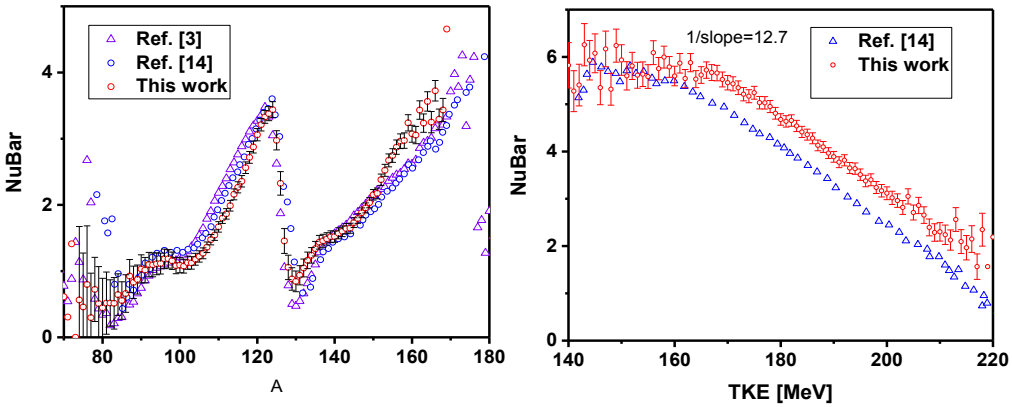

Fig. 4. The average PFN emission distribution mass dependence, measured in ^{252}Cf(sf) reaction in comparison with data from Refs. [3],[14 (on the left). The average PFN emission distribution dependence on FF TKE, measured in ^{252}Cf(sf) reaction with Q_{max}= ~239 MeV in comparison with data from Ref. [14] (on the right) Q_{max}= ~230.5 MeV.

was 0.725 m. Measurement was done with the data acquisition hardware and the software identical to that used in ^{235}U(n_{th},f) reaction investigation (except of WFD sampling frequency, which was 100 MHz). Data analysis was done using the same procedure as described above.

6 Conclusions and outlook

The average PFN emission was evaluated using the same data analysis software in the analysis of ^{235}U(n_{th},f) and ^{252}Cf(sf) reactions. The average PFN emission dependence on FF mass and TKE are presented in Fig. 3 and Fig. 4 for ^{235}U(n_{th},f) and ^{252}Cf(sf) respectively. The distributions for ^{252}Cf(sf) presented for FF recoil take into account effects of corrections according to Ref. [11]. It should be noted that the FF mass dependence of average neutron number also should be corrected according to formula (11) from Ref. [11], but this correction is very small for both in ^{235}U(n_{th},f) and ^{252}Cf(sf) reactions.

As it was pointed out in the review paper [12], use of a large neutron detector (with higher PFN detection efficiency), in many aspects is more preferable in PFN investigations. Bearing this in mind we developed new setup for PFN investigation, which would combine the properties of both detectors with high and low efficiency. New experimental setup

consists of a position sensitive twin fission chamber with capability to reconstruct the orientation of the fission axis in 3D [13] and to provide sufficient accuracy on the FF kinetic energy measurement. The twin chamber consists of a common cathode, where the fissile target can be located. Two segmented anodes are located at 40 mm distance symmetrically from the both sides of the cathode plane plain. Segmented anodes consist of triangular strips, electrically isolated from each other. Each strip is connected to the nodes of the resistive chain filter. Detailed operational principle of position sensitive ionization chamber, formulae for FF "charge centre-of -gravity" and FF orientation evaluation was provided in Refs. [8,13]. Fast neutron detector consist of 32 type VS-0499-100 scintillation detector modules of diameter 76 mm and 51 mm from SCIONIX HOLLAND BV (see Fig. 5). The setup is planned to be used in experiments in the end of this year at IREN which is a resonance neutron source facility in Dubna.

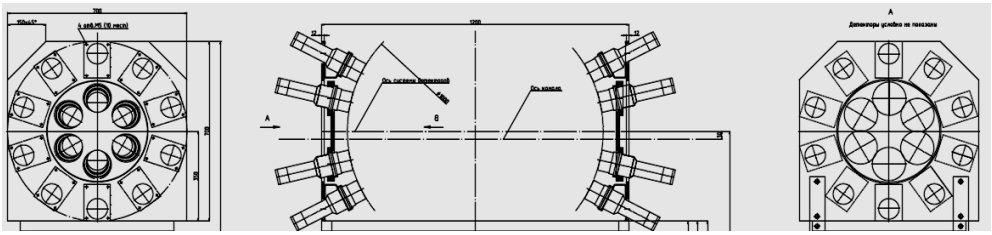

Fig. 5. Fast neutron detector composed of 32 liquid scintillation modules with position sensitive twin ionization chamber in centre (not shown in figure)

References

[1] A.A. Naqvi, F. Kappeler, and F. Dickmann, Phys. Rev. **C34**,218 (1986)
[2] A. Al-Adili, D. Tarrio, F.-J. Hambsch, A. Gook, K. Jansson, A. Solders, V. Rakopoulos, C. Gustavson, M. Lantz, A. Materrs, S. Oberstedt, A.V. Prokofiev, M. Viladi, M. Osterlund, and S. Pomp, *EPJ Web of Conferences* **122**, 01007 (2016)
[3] C. Budtz-Jorgensen and H.-H. Knitter, Nucl. Phys., **A490**, 307 (1988)
[4] C. Wagemans, *The Nuclear Fission Process*, CRC Press, Boca Raton , FL, 1991
[5] S. Zeynalov, O. Zeynalova, F.-J. Hambsch and S. Oberstedt, Bull. Russ. Acad. Sci.: Phys. **73**,506 (2009)
[6] Zeynalov, S., Hambsch, F.-J., Oberstedt, S., 2011. Jour. Korean Phys. Soc. **59**, 1396
[7] V.F. Apalin, Yu. N. Gtitsuk, I.E. Kutikov, V.I. Lebedev, and L.A. Mikaelyan, Nucl. Phys., **55**, 249 (1964).
[8] O. Zeynalova, Sh. Zeynalov, M. Nazarenko, F.-J. Hambsch, and S. Oberstedt, *AIP Conf. Proc*. **1404**, 325(2011)
[9] G. Knoll, *Radiation Detection and Measurement*, John Willey & Sons, Inc, Third edition, 2001
[10] H.R. Bowman, J.C.D. Milton, S.G. Thompson, and W.J. Swiatecki, Phys. Rev. **129** (1963) 2133
[11] A. Gavron, Nucl. Instrum. and Meth., **115** (1974) 99
[12] H. Nifenecker, C. Signarbieux, R. Babinet, J. Poitou, *Neutron and gamma emission in fission*, IAEA-SM-174/207
[13] Sh. Zeynalov, P. Sedyshev, O. Sidorova, V. Shvetsov, Applications of Nuclear Techniques (CRETE17), *International Journal of Modern Physics: Conference Series*, Vol. **48** (2018) 1860123.
[14] A. Gook, F.-J. Hambsch, and M. Vidali, Phys. Rev. C **90**, 064611 (2014)